

The Optical Gravitational Lensing Experiment. BVI Maps of Dense Stellar Regions. I. The Small Magellanic Cloud*

A. Udalski¹, M. Szymański¹, M. Kubiak¹,
G. Pietrzyński¹, P. Woźniak², and K. Żebruń¹

¹Warsaw University Observatory, Al. Ujazdowskie 4, 00-478 Warszawa,
Poland

e-mail: (udalski,msz,mk,pietrzyn,zebrun)@sirius.astrouw.edu.pl

²Princeton University Observatory, Princeton, NJ 08544-1001, USA
e-mail: woźniak@astro.princeton.edu

ABSTRACT

We present three color, *BVI* maps of the Small Magellanic Cloud. The maps contain precise photometric and astrometric data for about 2.2 million stars from the central regions of the SMC bar covering ≈ 2.4 square degrees on the sky. Mean brightness of stars is derived from observations collected in the course of the OGLE-II microlensing search from about 130, 30 and 15 measurements in the *I*, *V* and *B*-bands, respectively. Accuracy of the zero points of photometry is about 0.01 mag, and astrometry 0.15 arcsec (with possible systematic error up to 0.7 arcsec). Color-magnitude diagrams of observed fields are also presented.

The maps of the SMC are the first from the series of similar maps covering other OGLE fields: LMC, Galactic bulge and Galactic disk. The data are very well suited for many projects, particularly for the SMC which has been neglected photometrically for years. Because of potentially great impact on many astrophysical fields we decided to make the SMC data available to the astronomical community from the OGLE Internet archive.

Key words: *Magellanic Clouds – Surveys – Catalogs – Techniques: photometrics*

1 Introduction

The Optical Gravitational Lensing Experiment (OGLE) is a long term observing project which started in 1992 as the search for microlensing events

*Based on observations obtained with the 1.3 m Warsaw telescope at the Las Campanas Observatory of the Carnegie Institution of Washington.

in our Galaxy with the ultimate goal of providing information about the dark unseen matter (Udalski *et al.* 1992). In 1993 the first ever observed microlensing event toward the Galactic bulge was detected. In total about 20 microlensing events were found during the first phase of the project which ended in 1995 (Udalski *et al.* 1994, Woźniak and Szymański 1998).

Starting from January 1997 the OGLE project entered its second phase – OGLE-II. With a new, dedicated 1.3-m Warsaw telescope located at the Las Campanas Observatory, the observing capabilities of the OGLE project increased by a factor of 30 (Udalski, Kubiak and Szymański 1997). New targets, namely the Large and Small Magellanic Clouds, new fields in the Galactic bulge and Galactic disk have been added to the list of regularly observed regions of the sky.

After the first year of observations large databases of the observed targets have been created and first microlensing events have been detected (Udalski and Szymański 1998). The OGLE project photometric observations are collected in the standard *BVI*-bands which makes them very well suited not only for microlensing but also for many side projects. For instance, photometry of the LMC and SMC has already been used for a new distance determination to both Magellanic Clouds (Udalski *et al.* 1998, Udalski 1998).

In this paper, first of the series, we present the *BVI* maps of dense stellar regions in the SMC observed in the course of the OGLE-II project. The maps provide *BVI*-band photometry of all stellar objects detected in observed fields and in the case of the SMC contain well calibrated photometry and astrometry of about 2.2 million stars from the central regions (≈ 2.4 square degree) of the SMC bar. The data are used to construct color-magnitude diagrams (CMDs) of observed fields revealing many subtle features of stellar populations in the SMC.

Presented maps can be a very useful tool for many astronomical projects. For instance, a unique catalog of clusters in the SMC with accurate color-magnitude diagrams follows this paper (Pietrzyński *et al.* 1998). The SMC observations with the modern, precise techniques are rare and those which can be found in the literature concentrate on particular objects. The maps contain a full variety of objects including field stars and clusters located in different parts of the SMC and therefore are ideal for comparisons of stellar populations in different regions of the SMC.

Bearing in mind potential impact of the OGLE photometric data on our understanding of the SMC and other OGLE objects, we decided to make these data available to the astronomical community. At the end of this paper we provide information how to obtain the SMC maps. In the next papers

of this series the LMC and Galactic bulge maps will be gradually released.

In subsequent Sections we describe observations, reduction and calibration techniques used to construct the maps. Then results of accuracy and completeness tests are presented. Finally, we show CMDs of all our fields in the SMC.

2 Observations

All observations presented in this paper were carried out with the 1.3-m Warsaw telescope at the Las Campanas Observatory, Chile, which is operated by the Carnegie Institution of Washington, during the second phase of the OGLE experiment. The telescope was equipped with the "first generation" camera with the SITe 2048×2048 CCD detector. The pixel size was $24 \mu\text{m}$ resulting in $0.417 \text{ arcsec/pixel}$ scale. The observations of the SMC were performed in the "slow" reading mode of the CCD detector with the gain $3.8 \text{ e}^-/\text{ADU}$ and readout noise $\approx 5.4 \text{ e}^-$. Details of the instrumentation setup can be found in Udalski, Kubiak and Szymański (1997).

Observations of the SMC started on June 26, 1997. As the microlensing search is planned to last for a few years, observations of selected fields will be continued during next few seasons. In this paper we present data collected before the end of the first SMC season – Mar. 4, 1998. Observations were carried out in the driftscan mode. In this mode the CCD detector columns are aligned along the drift direction and the detector is read continuously with the rate synchronized with the drift rate of the star. As a result much larger areas can be observed with a single chip than in the normal, still frame mode. Also the dead time for detector reading is avoided. The images are rectangular with the width equal to the width of the CCD detector and the length proportional to the scanning time. For technical reasons – handling of large data files – OGLE driftscans are limited to 8192 lines which produces images of 2048×8192 pixel size ($\approx 34 \text{ MB}$ raw image). The OGLE driftscans are made with the drift along the meridian (*i.e.*, declination) direction. In this way any region of the sky is accessible for observations including the Magellanic Clouds located at high southern declinations. The drift of stars is forced by tracking the telescope in both axes: normal tracking in RA and additional tracking in declination. The declination tracking rate determines the effective exposure time which in the case of the SMC is 125 sec, 174 sec and 237 sec for the *I*, *V* and *B*-bands, respectively. Very sensitive CCD detector allows to obtain good photometry

down to $V \approx 21.5$ mag even with such relatively short exposure times.

Observations are made in three bands: B , V and I . Because of microlensing observing strategy, the vast majority of observations is collected in the I -band with some additional measurements in the B and V -bands. Standard set of glass Schott filters is used, closely approximating the standard BVI system.

Because of large stellar density in the OGLE-II main targets, the observations are limited to very good seeing conditions only, in order to ensure good photometry. Typical median seeing of presented data set is about 1.25 arcsec in the I -band with the best images reaching 0.8 arcsec. It should be noted that the active driftscans with open loop (no guiding) tracking in two axes give always slightly worse seeing because of inaccuracies in tracking etc. Observations of the SMC are usually stopped when the seeing exceeds 1.8 arcsec.

11 driftscan fields were selected in the SMC. They cover practically all dense regions of the SMC bar. Fig. 1 presents the picture of the SMC from the Digitized Sky Survey CD-ROMs with contours of our fields. Coordinates of the center of each field are given in Table 1. Each of the fields covers $\approx 14.2 \times 57$ arcmin on the sky (≈ 0.22 square degree). Fields are shifted in declination to follow the location of the center of the SMC bar on the sky. Neighboring fields overlap by about 1 arcmin for calibration of photometry and astrometry purposes. In the next observing seasons additional fields will be added to those listed in Table 1 to cover practically entire SMC.

During the first observing season about 100–150 observations in the I -band were collected, depending on the field. For two fields, SMC_SC5 and SMC_SC6 a few additional measurements were collected earlier, in January 1997. Number of B and V observations is smaller – about 15 and 30 per field, respectively. It is though, large enough to derive precise photometry of objects in these bands.

3 Photometric Reductions

3.1 The OGLE Data Pipeline

When a new frame is collected it is automatically intercepted by the OGLE photometric data reduction pipeline. All reductions are performed almost in real time at the telescope.

In the first step preliminary reductions are performed – debiasing, and flat-fielding based on regularly collected twilight sky flat-field and bias im-

Table 1
Equatorial coordinates of the SMC fields

Field	RA (J2000)	DEC (J2000)
SMC_SC1	0 ^h 37 ^m 51 ^s	−73°29′40″
SMC_SC2	0 ^h 40 ^m 53 ^s	−73°17′30″
SMC_SC3	0 ^h 43 ^m 58 ^s	−73°12′30″
SMC_SC4	0 ^h 46 ^m 59 ^s	−73°07′30″
SMC_SC5	0 ^h 50 ^m 01 ^s	−73°08′45″
SMC_SC6	0 ^h 53 ^m 01 ^s	−72°58′40″
SMC_SC7	0 ^h 56 ^m 00 ^s	−72°53′35″
SMC_SC8	0 ^h 58 ^m 58 ^s	−72°39′30″
SMC_SC9	1 ^h 01 ^m 55 ^s	−72°32′35″
SMC_SC10	1 ^h 04 ^m 51 ^s	−72°24′45″
SMC_SC11	1 ^h 07 ^m 45 ^s	−72°39′30″

ages. It should be noted that the driftscan mode flat-fields are one-dimensional line which is usually an average of a few thousand lines (depending on the length of the calibration driftscan flat-field image) and thus determined very precisely.

After the frame is de-biased and flat-fielded it is sent to the second stage reduction procedures which derive photometry of stars on the image. The photometry is calculated with the modified version of the DOPHOT photometry program (Schechter, Saha and Mateo 1993). Because of significant variations of the Point Spread Function (PSF) across the image caused by some inaccuracies of the telescope tracking and variable seeing in different moments of scanning, photometry reductions are performed on the 64 sub-frames of 512×512 pixel size on which the PSF can be assumed as constant in the first approximation. The DOPHOT program is run in the so called fixed position mode, that is an input list of positions of objects in a given field, generated in advance, is provided to the program. Coordinates from this list are transformed to fit the coordinates of the current frame and fixed for PSF photometry fitting. This mode is much faster and more accurate than the regular mode, in particular when the seeing of the frame is worse.

The input list of coordinates comes from the so called template image which is one of the best images of the entire data set for a given field and

filter taken at the possibly best seeing conditions. Positions of objects from the template images are obtained from photometric reductions with a special procedure based on regular and fixed mode reductions with the DOPHOT program. Photometry of each subframe of the template image is tied based on photometry in overlapping regions between subframes (for template reduction somewhat larger subframes are cut from the template image to reach 100 pixel overlap). Photometry of the template image is further treated as the reference instrumental photometry for the entire data set. Template coordinate lists for the B and V -bands are generated in similar way with the exception that positions of objects in these frames are fitted first with those of the I -band template image. In this way position of the star is always the same in the list of each band photometry which makes further data handling much easier.

When reductions of all subframes of a given image are done, photometry of each subframe is tied to that of the reference template subframe and results of photometry are stored in compact binary format in disk files. The process of reductions: dividing to subframes, reductions, correction of the zero points etc. is performed fully automatically. The amount of CPU of the system is sufficient to perform photometric reductions of all frames collected during the night (50–70 driftscans) within 24 hours.

3.2 Transformation to the Standard System

Several Landolt (1992) fields were observed during about 30 photometric nights to derive transformation of our instrumental magnitudes in the template photometric system to the standard BVI system. Based on a few hundreds of measurements of standard stars the following mean transformation was derived:

$$\begin{aligned}
 B &= b - 0.041 \times (B - V) + \text{const}_B \\
 V &= v - 0.002 \times (V - I) + \text{const}_V \\
 I &= i + 0.029 \times (V - I) + \text{const}_I \\
 B - V &= 0.959 \times (b - v) + \text{const}_{B-V} \\
 V - I &= 0.969 \times (v - i) + \text{const}_{V-I}
 \end{aligned} \tag{1}$$

where lower case letters b, v, i denote the aperture magnitudes normalized to 1 sec exposure time. The transformation coefficients are the mean for the entire season and were determined on a few nights when number of measurements of standard stars was large. The zero points and extinction

coefficients (when impossible, mean extinction values were used) were determined individually for each night. Residuals between fitted magnitudes of standard stars and observed ones did not exceed 0.02–0.03 mag.

As can be seen the transformation coefficients are close to zero for magnitude or one for color transformations, thus indicating that our instrumental system very well approximates the standard one and transformation errors are small. As the first step to convert our instrumental system to the standard one, aperture corrections to the template magnitudes were derived. A special procedure was written, based on the DOPHOT program, which reduces each subframe of a given image in analogous way as during normal reductions, selects bright stars well separated from neighboring stars which could contaminate their photometry and calculates the aperture magnitude for every selected star removing all remaining objects from the frame. About 10–50 aperture stars were usually used in each of the 64 subframes of a given image. The median of aperture corrections derived from these stars was adopted as the aperture correction of a given subframe. Next, the "total correction" for each subframe of a given image was calculated. This is defined as the sum of its aperture correction, the transformation zero point, extinction correction and normalization to 1 sec exposure time. Then "total corrections" determined from about 25, 10 and 6 nights for the *I*, *V* and *B*-bands, respectively, were averaged producing an array of 64 mean "total corrections" for a given field and band. Typical mean error of the final "total correction" values was less than 0.01 mag.

3.3 Final Databases of Results and BVI Maps of the SMC

"Total corrections", determined as described in the previous Section, were used to convert the template photometric system of each field and filter to the instrumental system very close to the standard one (the difference involves only color terms of Eqs. (1)). At this stage databases of photometric results were created and the appropriate "total corrections" were simply added to the template photometric system magnitudes when databases were filled up. The databases used are very similar to those developed for the OGLE-I phase of the project (Szymański and Udalski 1993) with some slight improvements and modifications. They contain all individual photometric measurements in the system close to the standard one (no color terms) and all basic information about each frame: heliocentric Julian date, exposure time, mean seeing and its standard deviation, frame grade etc. Entire database for a given field and filter consists of two parts – that of stars

detected on the template frame and that of "new" objects. In this paper we limit ourselves to the template objects only. The databases of the SMC contain approximately 2.25 million objects. The vast majority of them are objects classified by the DOPHOT program as stellar.

Table 2
Number of stellar objects in the SMC maps

Field	No of stellar objects
SMC_SC1	120002
SMC_SC2	107326
SMC_SC3	240045
SMC_SC4	198201
SMC_SC5	319850
SMC_SC6	326367
SMC_SC7	268006
SMC_SC8	211115
SMC_SC9	176832
SMC_SC10	140589
SMC_SC11	120932

When the databases of photometric results were created for each field and filter for our SMC fields, the final *BVI*-band maps of the SMC were constructed. First, measurements of each star were averaged with 5σ rejection algorithm in each band. Then color term transformation corrections were calculated and finally the standard system magnitudes were derived. Only magnitudes derived from more than 40, 10 and 5 good measurements in the *I*, *V* and *B*-bands, respectively, were listed in the final maps of the SMC. Good measurement was defined as the one with the stellar type object returned by the DOPHOT program and the error returned by DOPHOT not exceeding 1.6 median of the errors from the entire set of measurements of a given star. Final number of objects included in the SMC maps is given in Table 2.

Table 3 presents sample data of the final map for the SMC_SC4 field. The following data are provided: star number in the database, equatorial coordinates (RA and DEC, J2000) of the star, x and y positions in the *I*-band template image, magnitudes: V , $B - V$, $V - I$, B and I , number of

Table 3
Sample of data from the *BVI* map of the field SMC_SC4

Star no	RA (J2000)	DEC (J2000)	<i>X</i>	<i>Y</i>	<i>V</i>	<i>B</i> − <i>V</i>	<i>V</i> − <i>I</i>	<i>B</i>	<i>I</i>	N_{ok}^B	N_{bad}^B	σ^B	N_{ok}^V	N_{bad}^V	σ^V	N_{ok}^I	N_{bad}^I	σ^I
1	0 ^h 45 ^m 51 ^s :29	−73°35′05″.7	348.38	89.42	14.709	0.198	0.299	14.907	14.410	15	0	0.090	21	1	0.019	121	0	0.017
2	0 ^h 45 ^m 20 ^s :39	−73°35′00″.3	31.48	99.25	14.713	0.785	1.013	15.501	13.698	11	0	0.074	20	0	0.066	67	0	0.038
3	0 ^h 46 ^m 02 ^s :27	−73°34′50″.6	460.56	126.77	16.458	1.939	2.380	18.405	14.076	17	0	0.144	28	0	0.113	118	0	0.044
4	0 ^h 45 ^m 43 ^s :54	−73°34′49″.7	268.57	127.37	15.499	1.227	1.173	16.731	14.324	17	0	0.065	29	0	0.028	122	0	0.016
5	0 ^h 45 ^m 26 ^s :73	−73°34′21″.6	95.49	193.50	16.853	−	2.551	−	14.299	0	0	−	24	0	0.080	114	0	0.066
6	0 ^h 45 ^m 59 ^s :66	−73°32′41″.9	431.42	437.67	15.779	1.400	1.333	17.183	14.444	18	0	0.034	26	0	0.018	124	0	0.017
7	0 ^h 45 ^m 42 ^s :92	−73°34′47″.5	262.12	132.43	16.829	1.795	1.713	18.631	15.115	18	0	0.106	27	0	0.028	118	0	0.018
8	0 ^h 45 ^m 25 ^s :84	−73°34′39″.5	86.88	150.20	16.633	1.322	1.437	17.960	15.195	17	0	0.058	27	1	0.023	114	0	0.015
10	0 ^h 45 ^m 39 ^s :50	−73°33′59″.7	226.00	247.82	15.900	1.245	1.267	17.150	14.632	17	1	0.014	28	1	0.012	122	0	0.008
11	0 ^h 45 ^m 41 ^s :06	−73°33′53″.5	241.91	262.99	14.956	−0.038	0.202	14.918	14.754	17	0	0.027	29	0	0.028	123	0	0.010
12	0 ^h 45 ^m 47 ^s :12	−73°33′02″.2	303.06	387.49	16.943	1.966	1.654	18.916	15.287	16	0	0.075	25	0	0.015	122	0	0.017
13	0 ^h 45 ^m 20 ^s :77	−73°32′54″.5	32.21	403.44	16.053	1.049	1.234	17.106	14.817	14	0	0.044	23	0	0.023	80	0	0.025
14	0 ^h 45 ^m 35 ^s :84	−73°32′54″.8	187.00	404.25	16.342	1.020	1.146	17.366	15.195	18	0	0.033	27	1	0.013	123	0	0.017
15	0 ^h 45 ^m 51 ^s :99	−73°32′25″.2	352.35	477.23	16.777	1.527	1.485	18.309	15.290	18	0	0.062	29	0	0.017	128	0	0.020
17	0 ^h 45 ^m 36 ^s :38	−73°35′16″.6	195.74	61.58	−	−	−	18.932	15.759	13	0	0.097	0	0	−	107	1	0.019
18	0 ^h 45 ^m 57 ^s :08	−73°34′48″.0	407.38	132.61	16.133	0.510	0.639	16.645	15.493	17	0	0.119	29	0	0.081	123	0	0.060
19	0 ^h 45 ^m 26 ^s :80	−73°34′37″.0	96.60	156.20	17.420	1.158	1.406	18.582	16.012	18	0	0.031	28	1	0.030	118	0	0.022
20	0 ^h 45 ^m 20 ^s :75	−73°34′11″.9	33.93	216.24	17.190	1.397	1.493	18.593	15.696	14	0	0.039	24	0	0.024	87	0	0.021
21	0 ^h 45 ^m 59 ^s :13	−73°34′02″.3	427.53	243.16	17.129	1.488	1.463	18.622	15.664	17	0	0.044	28	0	0.012	124	0	0.012
22	0 ^h 46 ^m 07 ^s :12	−73°34′00″.3	509.43	248.73	16.852	1.625	1.477	18.483	15.374	18	0	0.082	28	0	0.019	126	0	0.017

observations, number of rejected observations and standard deviation of the mean magnitude for B , V and I -bands, respectively. Such maps for all our fields are available to the astronomical community (see Section 7).

4 Astrometry

To convert positions of stars to the equatorial system the pixel coordinate system of the I -band template image for each field was transformed to the equatorial system using the Digital Sky Survey (DSS) images.

The procedure consists of the following steps. First, FITS image, somewhat larger than the area of a given field, is extracted from the DSS CD-ROMs. Then, the "autofind" program is run on that frame. It finds all objects brighter than selected threshold and calculates a centroid of each detected object. Now, the main transformation program is run. First, it converts the (x, y) coordinates of each star from the DSS image to RA and DEC based on prescription and procedures provided with the DSS distribution. Then (RA, DEC) of each star are transformed with simple trigonometric formulae to (x', y') coordinates of the Cartesian system on the plane tangent to the celestial sphere at the center of a given field. Finally, transformation between (x', y') coordinates and pixel coordinate system of the I -band template image follows. The transformation between those two systems of coordinates is relatively simple and third order polynomials are sufficient to achieve good accuracy. The transformation is calculated in a few iterations with decreasing critical radius within which objects are treated as identical. The final critical radius is 0.75 arcsec. About 3000–8000 stars in the SMC fields were used for transformation depending on stellar density of the field.

5 Data Tests

5.1 Photometry

To assess quality of photometry a few tests were performed. First, we compared photometry of the same stars located in the overlapping regions between fields. As the overlapping regions extend along the length of the image we compared the magnitude differences of stars on both frames as a function of line number. Figs. 2, 3 and 4 present plots "magnitude difference *vs.* CCD line number" for fields located in the west, center and east regions of the SMC (SMC_1–2, SMC_5–6, and SMC_9–10) for filters B , V

and *I*. Similar plots for other fields look practically identical. As can be seen the photometry in overlapping regions of neighboring fields is in very good agreement. The mean difference is always below 0.01 mag indicating that our calibration procedures were correct.

In the second test we compared our photometry with other reliable measurements from the literature. Unfortunately good quality observations of the SMC with modern techniques are rare. We limited our comparison mostly to CCD measurements, as only those can be reliable in crowded fields of the SMC. We found the following past observations of the SMC:

- CCD photometry of NGC 346 was published by Massey, Parker and Garmany (1989). Only part of this cluster is located in the SMC_SC8 field. The mean difference between the OGLE and Massey, Parker and Garmany (1989) photometry is $\Delta V = 0.003 \pm 0.032$ mag (42 stars) and $\Delta(B - V) = -0.022 \pm 0.033$ mag (31 stars).
- CCD photometry of NGC 330 (SMC_SC7 field) was obtained by Walker (Caloi *et al.* 1993). Photometry of Walker is in good agreement with more recent photometry of Vallenari, Ortolani and Chiosi (1994). The mean difference between the OGLE and Walker photometry is $\Delta V = -0.002 \pm 0.020$ mag and $\Delta(B - V) = 0.040 \pm 0.014$ mag (9 stars).
- CCD photometry of the field around HV 1876 (SMC_SC9 field) variable star (Jensen, Clausen and Giménez 1988). The mean difference between the OGLE and Jensen, Clausen and Giménez (1988) photometry of proposed standard stars is $\Delta V = 0.004 \pm 0.030$ mag and $\Delta(B - V) = 0.002 \pm 0.018$ mag.
- CCD photometry of the field around HV 2016 (SMC_SC11 field) variable star (Jensen, Clausen and Giménez 1988). The mean difference between the OGLE and Jensen, Clausen and Giménez (1988) photometry of proposed standard stars is $\Delta V = -0.007 \pm 0.011$ mag and $\Delta(B - V) = 0.015 \pm 0.006$ mag.
- Photoelectric photometry sequence around NGC 419 (SMC_SC11 field) was obtained by Wenderoth *et al.* (1994). Although we do not trust photoelectric photometry in such dense fields because of crowding we checked photometry of the brightest stars of that sequence which are still not saturated in our images. The mean difference between the OGLE and Wenderoth *et al.* (1994) photometry is $\Delta V = -0.007 \pm 0.010$ mag, $\Delta(B - V) = -0.059 \pm 0.013$ mag and $\Delta(V - I) = -0.001 \pm 0.032$ mag

- Finally we compared the I -band light curves of two "stable" variable stars from the NGC 330 region (SMC_SC7 field), namely Cepheid variables #389 and #952, observed by Sebo and Wood (1994) to those retrieved from the OGLE databases – Fig. 5. It can be seen that zero points of both photometries are in very good agreement confirming that OGLE zero points are determined correctly.

Summarizing, very good agreement of photometry derived independently in neighboring fields and comparison with reliable measurements from the literature indicate that our photometry is calibrated correctly. We estimate that the systematic error of our photometry should not exceed 0.01 mag.

5.2 Completeness

To assess completeness of our three color maps of the SMC we performed a series of artificial stars tests. We selected for tests 512×512 pixel subframes of each band template images of three fields. These fields are located in the east, center and west regions of the observed part of the SMC, namely SMC_SC1, SMC_SC6 and SMC_SC10 and represent the least and most dense regions of the SMC bar. Selected subframes cover the central, most dense part of each field.

To each subframe a number of artificial stars in randomly selected positions was added using a special software based on DOPHOT procedures. In order not to change crowding of the frame we added only 296 stars in each test with magnitude distribution as shown in column 1 of Table 4. Then we checked how many of them were recovered with our standard reduction pipeline treating the input and output star as identical if its difference of position and magnitude was smaller than 0.8 arcsec and ± 0.5 mag, respectively. One hundred such tests were performed for each subframe. The rate of recovered objects is listed in Table 4.

It is clear that down to $B \approx 20.0$, $V \approx 20.5$ and $I \approx 20.0$ detection completeness is very high and then it fades gradually reaching $\approx 50\%$ at $B \approx 21.2$, $V \approx 21.5$ and $I \approx 21.0$ for the least dense fields. This figures might be assumed as limiting magnitudes of our survey. As expected completeness is somewhat lower for the most dense field SMC_SC6.

Our maps contain only objects which were detected in the I -band templates. Therefore the I -band completeness tests correspond to completeness of our maps. Additional objects present only in V and/or B -band templates as well as objects from "new" databases were not included in the maps. We

Table 4
Completeness of the SMC maps

Stars per bin	<i>B</i>	Completeness			<i>V</i>	Completeness			<i>I</i>	Completeness		
		SC_1	SC_6	SC_10		SC_1	SC_6	SC_10		SC_1	SC_6	SC_10
2	14.0	100.0	100.0	100.0	14.5	100.0	99.0	100.0	13.8	100.0	100.0	100.0
5	14.5	100.0	99.6	100.0	15.0	99.6	100.0	99.8	14.3	99.4	100.0	99.8
7	15.0	99.4	99.7	99.9	15.5	99.9	99.4	100.0	14.8	100.0	99.9	99.9
10	15.5	99.6	99.3	99.7	16.0	100.0	99.3	99.3	15.3	99.8	99.4	99.9
12	16.0	99.0	99.7	99.7	16.5	99.6	99.3	99.5	15.8	99.6	99.3	99.5
15	16.5	98.7	98.8	99.8	17.0	99.1	98.5	99.3	16.3	99.9	99.5	99.8
17	17.0	98.8	98.4	99.0	17.5	98.8	98.6	99.1	16.8	99.5	99.1	98.9
20	17.5	97.9	98.4	99.7	18.0	98.8	97.8	98.7	17.3	99.5	98.8	99.1
22	18.0	98.1	96.7	98.7	18.5	98.0	96.0	97.3	17.8	98.7	97.5	98.4
25	18.5	97.2	94.5	98.2	19.0	97.2	93.0	96.1	18.3	98.5	95.1	98.0
27	19.0	97.1	90.9	96.7	19.5	94.4	90.3	95.0	18.8	98.2	93.6	96.4
30	19.5	94.7	83.7	95.0	20.0	93.5	86.3	92.0	19.3	96.8	89.3	95.9
32	20.0	91.7	74.8	89.1	20.5	89.5	78.9	87.2	19.8	95.2	84.8	93.2
35	20.5	87.0	58.9	79.6	21.0	78.8	65.0	76.0	20.3	91.8	72.4	85.8
37	21.0	77.9	37.4	33.1	21.5	53.0	42.9	56.4	20.8	76.7	42.1	55.3

estimate that only small percentage of objects was omitted.

5.3 Astrometry

Accuracy of our astrometric solutions was checked by comparison of coordinates of detected objects located in overlapping regions between fields. First, transformation between fields was derived and common objects were identified. Then, equatorial coordinates of each identified object were calculated based on transformations for both fields and the difference between the two. Finally, the mean difference and its standard error were calculated from the entire sample of identified pairs of stars (typically a few hundred objects). The mean difference of coordinates between fields was typically about 0.1–0.15 arcsec with the standard deviation of about 0.1–0.2 arcsec. This error is representative of internal error of our determination of equatorial coordinates.

To check possible systematic errors we compared fields with astrometric solutions based on different plates from the DSS. We repeated the above pro-

cedure comparing coordinates of fields determined from different plates of the DSS. In this case the mean difference was much larger, sometimes reaching 0.7 arcsec. This number might be assumed as the possible systematic error of the DSS coordinates system and thus of our equatorial coordinates.

6 Color-Magnitude Diagrams

Based on our three color maps of the SMC, we constructed composite color-magnitude diagrams for each of our fields. Figs. 6–16 present the $V-(B-V)$ and $V-(V-I)$ CMDs of all our fields in the SMC. Only 10–30% of stars were included in these Figures for clarity.

The CMDs of the SMC fields reveal in great detail main features known from previous studies: the main sequence, red giant branch with nicely pronounced red clump of giants, its vertical extension (similar to that observed in the LMC, *cf.* Zaritsky and Lin 1997, Beaulieu and Sackett 1998, Udalski *et al.* 1998) and asymptotic branch clump. Also many other fine features become recognizable due to large statistics of stars in these diagrams. It is obvious that our maps provide a unique tool for analysis of the wide variety of topics concerning the SMC and stars in general.

7 Conclusions

We release in this paper the three color, BVI -band maps of the SMC. The data contain photometry for about 2.2 million stars from the central parts of the SMC bar. The data are precisely calibrated, the mean magnitudes are determined from tens/hundreds of individual measurements. Our tests show that accuracy of the zero point of our photometry should be about 0.01 mag. Precise equatorial coordinates for all objects are determined from the DSS astrometric solution with internal accuracy of about 0.15 arcsec, and possible systematic errors of the DSS astrometric system up to 0.7 arcsec. Large number of photometric measurements used for determination of mean magnitudes makes our unique data a huge set of secondary photometric standards in the SMC.

In the next paper of this series similar data for the LMC bar fields observed during the OGLE-II project will be presented. Release of similar maps of the Galactic bulge is planned in the future.

The three color maps are available to the astronomical community from the OGLE archive <http://www.astrow.edu.pl/~ftp/ogle> and its mirror <http://www.astro.princeton.edu/~ogle> (or <ftp://astro.princeton.edu/ogle/ogle2/maps/smc>). Also *I*-band FITS template images of our fields are included. Due to large volume of data – about 400 MB, which is not always suitable for network transfers we also distribute the entire set of data on CD-ROMs for a small fee covering handling costs. Please contact *via* e-mail: cfpa@sirius.astrow.edu.pl. Usage of the data is allowed under the condition of proper acknowledgment to the OGLE project.

We provide these data in the most original form to avoid any additional biases. For instance we do not mask bright stars which often produce many artifacts, but such masking could potentially remove some interesting information on objects located close to bright stars. We do not remove objects which are located in overlapping areas between the neighboring fields. Cross-identification of these objects can be easily done based on provided equatorial coordinates.

Acknowledgements. We would like to thank Prof. Bohdan Paczyński for many encouraging discussions and help at all stages of the OGLE project. The paper was partly supported by the Polish KBN grant 2P03D00814 to A. Udalski. Partial support for the OGLE project was provided with the NSF grant AST-9530478 to B. Paczyński. We acknowledge usage of The Digitized Sky Survey which was produced at the Space Telescope Science Institute based on photographic data obtained using The UK Schmidt Telescope, operated by the Royal Observatory Edinburgh.

REFERENCES

- Beaulieu, J.P., and Sackett, P.D. 1998, *Astron. J.*, in press, (astro-ph/9710156).
 Caloi, V., Cassatella, A., Castellani, V., and Walker, A. 1993, *Astron. Astrophys.*, **271**, 109.
 Jensen, K.S., Clausen, J.V., and Giménez, A. 1988, *Astron. Astrophys. Suppl. Ser.*, **74**, 331.
 Landolt, A.U. 1992, *Astron. J.*, **104**, 372.
 Massey, P., Parker, J.W., and Garmany, C.D. 1989, *Astron. J.*, **98**, 1305.
 Pietrzyński, G., Udalski, A., Szymański, M., Kubiak, M., Woźniak, P., and Żebruń, K. 1998, *Acta Astron.*, **48**, 175.
 Schechter, P.L., Saha, K., and Mateo, M. 1993, *P.A.S.P.*, **105**, 1342.
 Sebo, K.M., and Wood, P.R. 1994, *Astron. J.*, **108**, 932.
 Szymański, M., and Udalski, A. 1993, *Acta Astron.*, **43**, 91.
 Udalski, A. 1998, *Acta Astron.*, **48**, 113.
 Udalski, A., Kubiak, M., and Szymański, M. 1997, *Acta Astron.*, **47**, 319.
 Udalski, A., and Szymański, M. 1998, *IAU Circ.*, #6901.

- Udalski, A., Szymański, M., Kałużny, J., Kubiak, M. and Mateo, M. 1992, *Acta Astron.*, **42**, 253.
- Udalski, A., Szymański, M., Stanek, K.Z., Kałużny, J., Kubiak, M., Mateo, M., Krzemiński, W., Paczyński, B., and Venkat, R. 1994, *Acta Astron.*, **44**, 165.
- Udalski, A., Szymański, M., Kubiak, M., Pietrzyński, G., Woźniak, P., and Żebruń, K. 1998, *Acta Astron.*, **48**, 1, (astro-ph/9803035).
- Vallenari, A., Ortolani, S., and Chiosi, C. 1994, *Astron. Astrophys. Suppl. Ser.*, **108**, 571.
- Wenderoth, E.,
Alvarado, F., Alcaino, F., and Liller, W. 1994, *Astron. Astrophys. Suppl. Ser.*, **106**, 253.
- Woźniak, P., and Szymański, M. 1998, *Acta Astron.*, **48**, 269.
- Zaritsky, D., and Lin, D.B.C. 1997, *Astron. J.*, **114**, 2545.

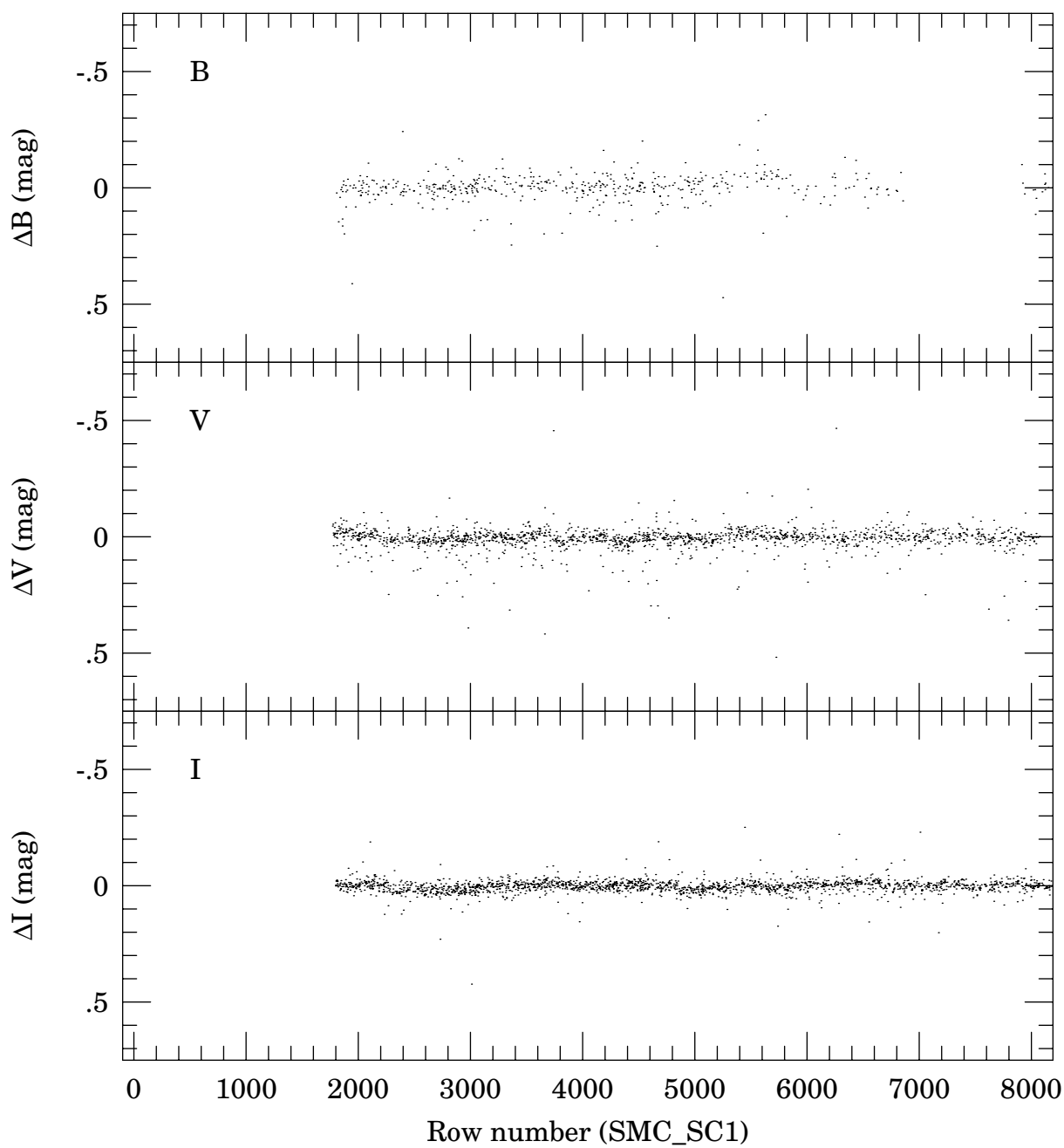
Figure Captions

- Fig. 1. OGLE-II fields in the SMC. North is up and East to the left.
- Fig. 2. Difference of magnitude in overlapping regions of fields SMC_SC2 and SMC_SC1.
- Fig. 3. Difference of magnitude in overlapping regions of fields SMC_SC6 and SMC_SC5.
- Fig. 4. Difference of magnitude in overlapping regions of fields SMC_SC10 and SMC_SC9.
- Fig. 5. Comparison of photometry of two Cepheid variables observed by Sebo and Wood (1994) and OGLE-II.
- Fig. 6. Color-magnitude diagrams of the SMC_SC1 field. About 20% stars from this field are plotted.
- Fig. 7. Color-magnitude diagrams of the SMC_SC2 field. About 30% stars from this field are plotted.
- Fig. 8. Color-magnitude diagrams of the SMC_SC3 field. About 13% stars from this field are plotted.
- Fig. 9. Color-magnitude diagrams of the SMC_SC4 field. About 13% stars from this field are plotted.
- Fig. 10. Color-magnitude diagrams of the SMC_SC5 field. About 10% stars from this field are plotted.
- Fig. 11. Color-magnitude diagrams of the SMC_SC6 field. About 10% stars from this field are plotted.
- Fig. 12. Color-magnitude diagrams of the SMC_SC7 field. About 13% stars from this field are plotted.
- Fig. 13. Color-magnitude diagrams of the SMC_SC8 field. About 20% stars from this field are plotted.
- Fig. 14. Color-magnitude diagrams of the SMC_SC9 field. About 20% stars from this field are plotted.
- Fig. 15. Color-magnitude diagrams of the SMC_SC10 field. About 20% stars from this field are plotted.
- Fig. 16. Color-magnitude diagrams of the SMC_SC11 field. About 30% stars from this field are plotted.

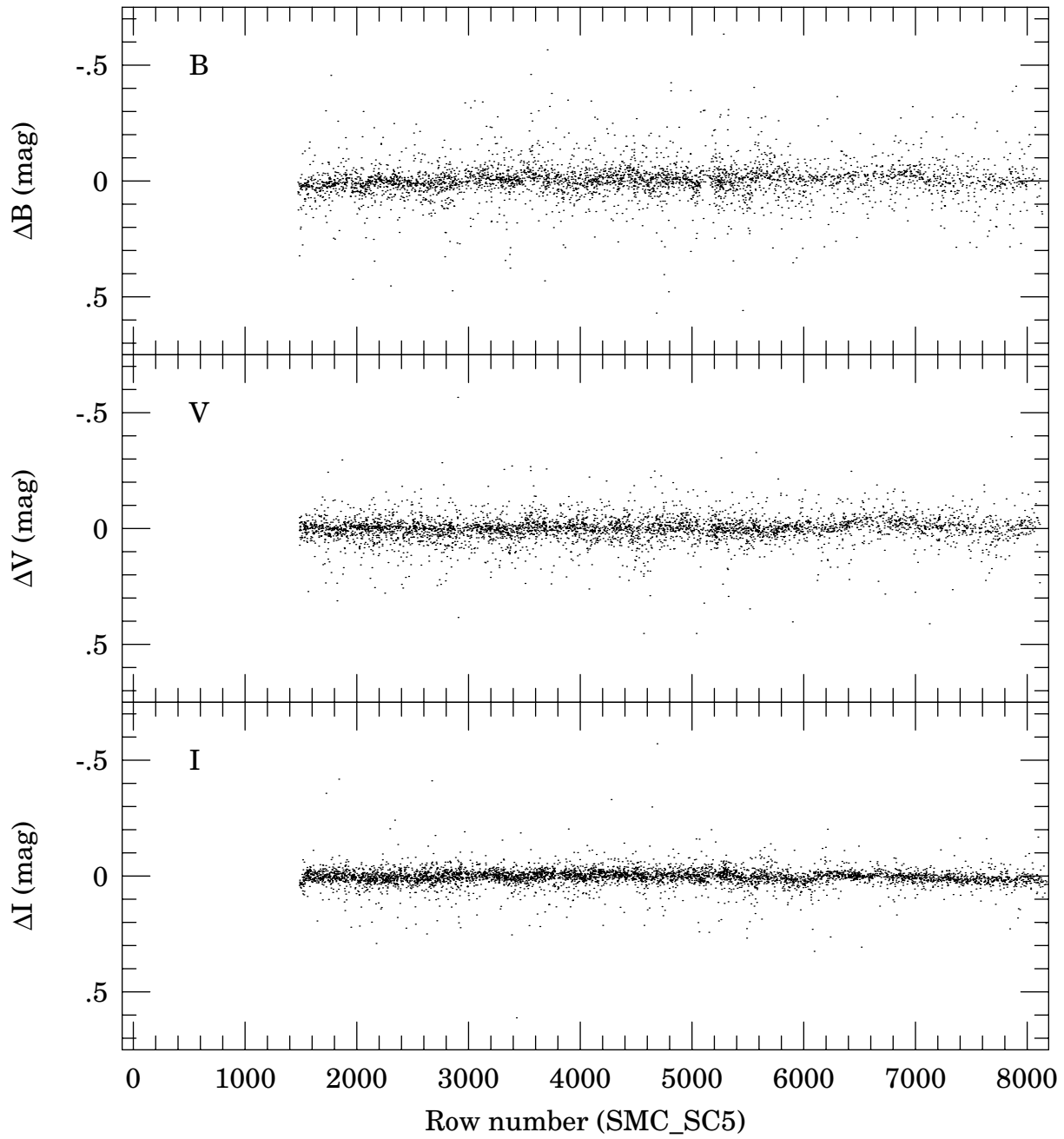
This figure "fig1.jpg" is available in "jpg" format from:

<http://arxiv.org/ps/astro-ph/9806313v2>

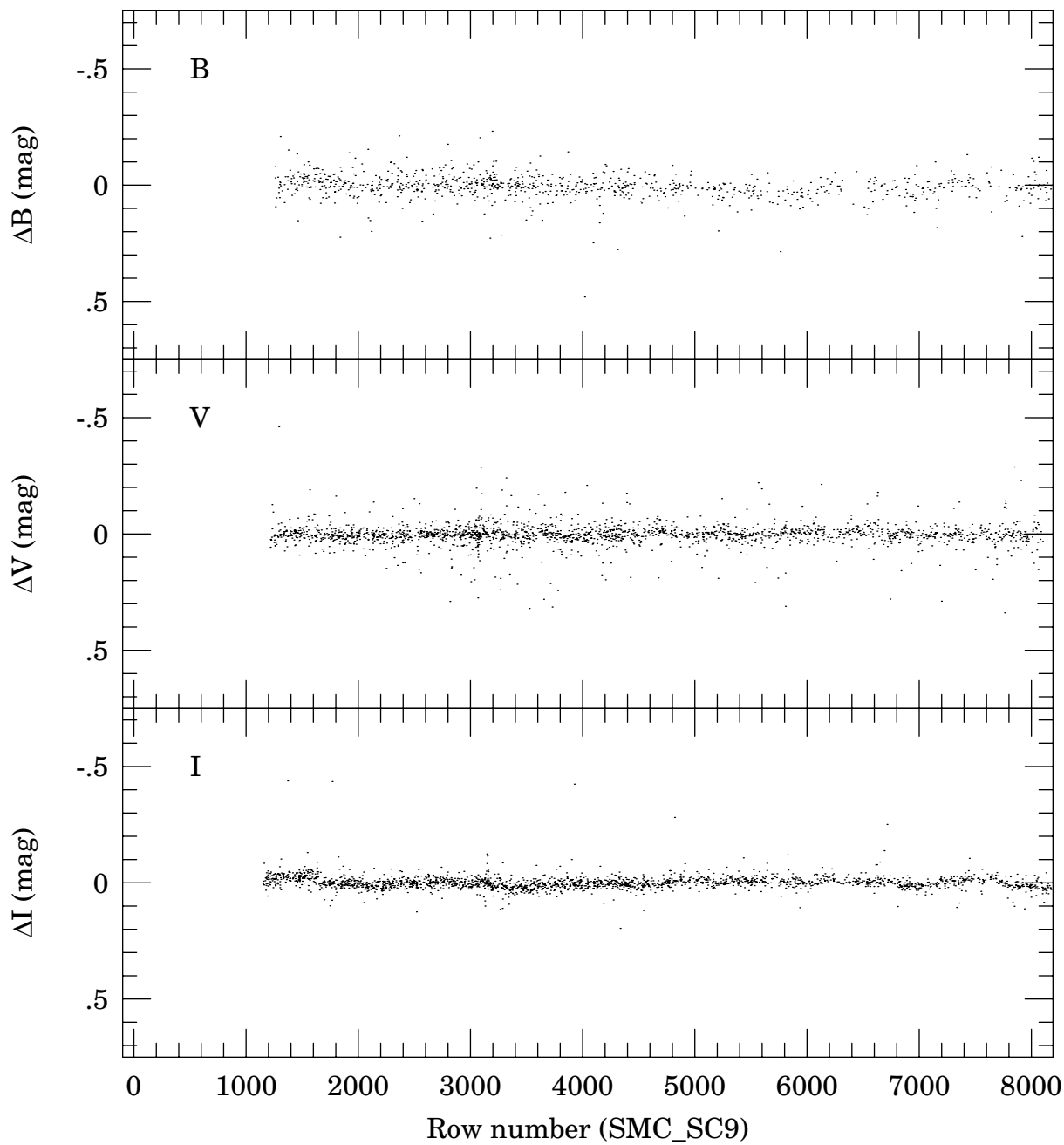
SMC_SC2 - SMC_SC1

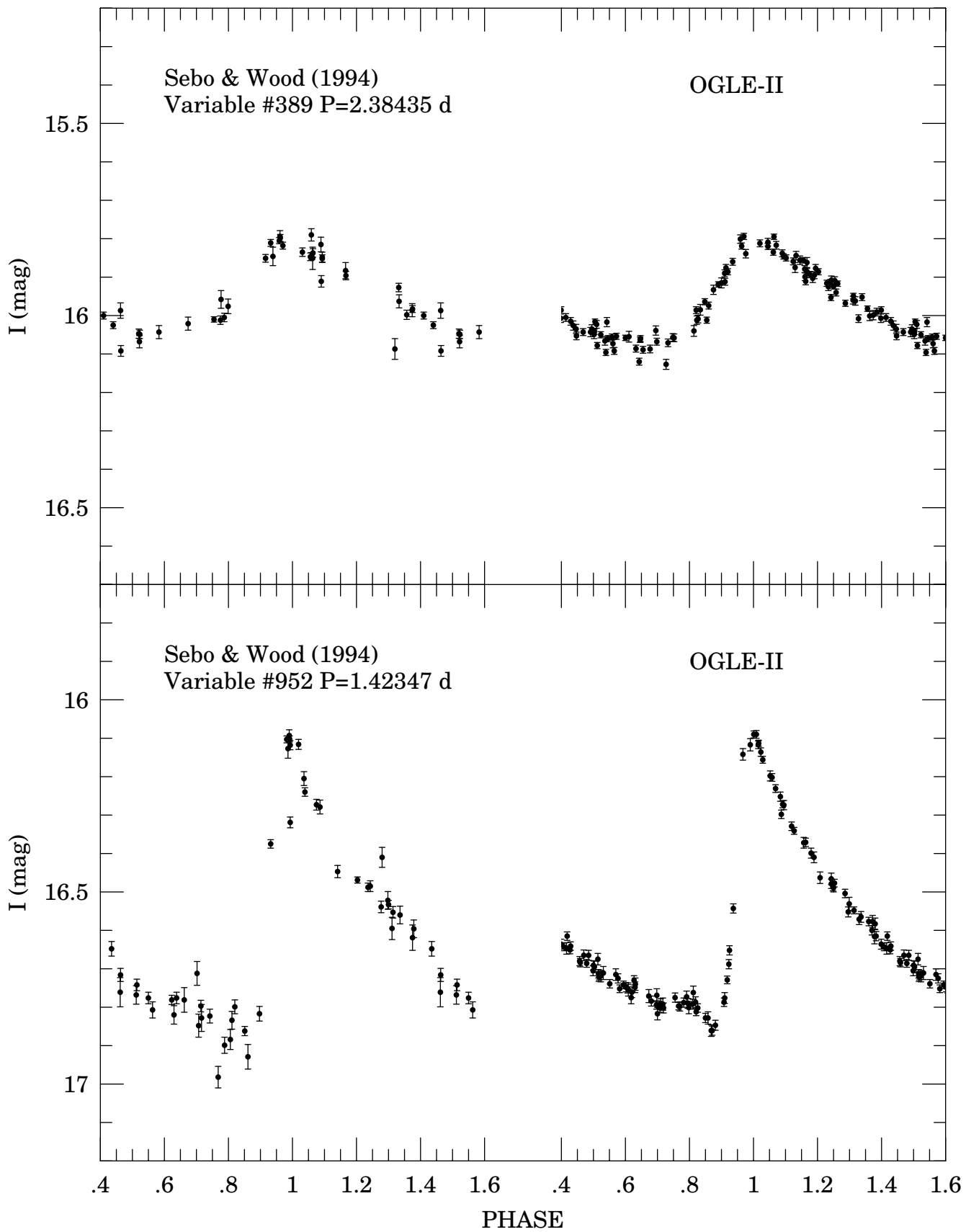


SMC_SC6 - SMC_SC5



SMC_SC10 - SMC_SC9





This figure "fig6.jpg" is available in "jpg" format from:

<http://arxiv.org/ps/astro-ph/9806313v2>

This figure "fig7.jpg" is available in "jpg" format from:

<http://arxiv.org/ps/astro-ph/9806313v2>

This figure "fig8.jpg" is available in "jpg" format from:

<http://arxiv.org/ps/astro-ph/9806313v2>

This figure "fig9.jpg" is available in "jpg" format from:

<http://arxiv.org/ps/astro-ph/9806313v2>